INNSPUB

International Journal of Biosciences | IJB |
ISSN: 2220-6655 (Print) 2222-5234 (Online)
http://www.innspub.net
Vol. 13, No. 4, p. 322-332, 2018

RESEARCH PAPER OPEN ACCESS

Kinetics and Mechanism of the Adsorption of water-soluble anticancer drug on iron oxide nanoparticles doped with ferromagnetic materials

Khalid Rashid*[1,2], Alvina Rafiq Butt[1], MunirAhmad[3], Muhammad Nafees[1], Salamat Ali[1], Muhammad Ikram[1] Uzma Sattar[2]

[1]*Materials and Nano Research Lab (MNRL), Department of Physics, Government College University, Lahore, Punjab, Pakistan*

[2]*Pakistan Council of Scientific and Industrial Research (PCSIR), Lahore, Punjab, Pakistan*

[3]*Medical Physics, Institute of Nuclear Medicine and Oncology (INMOL), Lahore, Punjab, Pakistan*

Key words: Doxorubicin, Ferromagnetic, Nanoparticles, Drug loading, Doping; specificity, Kinetics, Mechanism.

http://dx.doi.org/10.12692/ijb/13.4.322-332 Article published on October 30, 2018

Abstract

Pure and doped iron oxide as spherical nanocarriers for the anticancer drug was synthesized using simple and cost-effective co-precipitation technique. A variety of techniques as XRD- x-ray diffraction, EDX- energy dispersive x-ray spectroscopy, UV-Vis-ultraviolet visible spectroscopy, SEM- scanning electron microscope and TEM- transmission electron microscope were employed to the prepared ferromagnetic metal oxide- (Fe_3O_4) and Co and Ni doped ferromagnetic materials to check their structural, compositional and morphological properties. These metaloxides nanocarriers were incorporated with ananti-cancer marker (doxorubicin) and loading capabilities were observed. The observed data was analyzed on different kinetics models. It was found that the drug loading capability of Cobalt doped Fe_3O_4 nanocarriers is higher relative to other carriers observed data was matched exactly with Lagergren Pseudo-first-order, Pseudo-second-order, Elovich equation and Intra-particle diffusion models.

* **Corresponding Author:** Khalid Rashid ✉ khalid_pcsir@yahoo.com

Introduction

Cancer is an ill health that includes over 200 diseases and is associated by un-controlled spreading and proliferation of diseased cells. Although the conventional therapies such as chemotherapy, radiotherapy and surgery are widely accepted with some adverse effects are still to be considered. Especially, chemotherapy needs to save the organs at risk and to reach the tumor sites in suitable quantities. However, the hostile effects can be elucidated by advancing certain aspects as by introducing the nanoparticles can be used nanocarriers, with a great extent of loading capability, in drug delivery mechanisms (Ahmd *et al.*, 2012). Nanoparticles (NPs) are being utilized in transporting vaccines, nucleotides, proteins and conventional drugs owning to significant potency to invade the blood barriers. The transport mechanism can be modified by appropriate functionalization of NPs that possibly improve specific binding with organs, drug kinetics, drug-carrying capabilities and excretions (Parveen, Misra, & Sahoo, 2012).

NPs are also implied in pharmaceutical sciences to minimize the adversity drugs, conversely of induced hazards are not yet clear and still under investigation. For instance, inhalation toxicity of NPs may potential influence on exposure to different organs (Jatariu, Peptu, Popa, & Indrei, 2009; De Jong & Borm, 2008). Optimistically, the transportation through blood barriers may introduce new paths of drug delivery to approach the brain. Various biological substances as gelatin, albumin, phospholipids, polymers etc. are under consideration to produce nanocarriers (NPs) for delivery mechanisms. It is well known that intracellular and tissue interactions are highly dependent upon nanoparticle formulations (De Jong & Borm, 2008; Dilnawaz, Singh, Mohanty, & Sahoo, 2010; Kim, Zhang, Voit, Rao, & Muhammed, 2001). Superparamagnetic iron oxide nanoparticles (SPIONs) are most attractive and favorable in delivery applications because of surface architecture and conjugation with targeting drugs, ligands or proteins via external magnets (De Jong & Borm, 2008; Ito, Shinkai, Honda, & Kobayashi, 2005; Mahmoudi, Sant, Wang, Laurent & Sen, 2011; Neuberger, SchApf, Hofmann, Hofmann, & von Rechenberg, 2005).

The controlled drug delivery system (DDS) is potential route over the customary drug transportation. The drug accumulates on approaching at target sites while minimizing unavoidable side effects. The increase in drug accumulation is caused to reduce the desired amount of drug dose. Nanocarriers are designed to prolong the therapeutic effects of drug at focal site in parallel to keep the healthy tissues safe from the drug concentration (Kale & Torchilin, 2007; Kohay *et al.*, 2017; Peer *et al.*, 2007; Wilczewska, Niemirowicz, Markiewicz, & Car, 2012). During this advanced therapy, be cautious about the ratio between drug concentration, drug dose and therapeutic toxic effects. Numerous nanostructures, as polymers, liposomes, dendrimers, carbon materials and magnetic nanoparticles, are assessed as carriers in DDS (Khoee, Bafkary, & Fayyazi, 2017).

Doxorubicin (DOX) is one of the most efficient and widely used anticancer drugs that fight against many kinds of tumor cells. It has very serious side effects on kidney, heart and liver tissues. To get over these aspects, some appropriate vectors should be introduced to deliver DOX to minimize their side effects (Javed *et al.*, 2015; Chen *et al.*, 2016).

In this work, pure and various ratios of (Co and Ni) doped Fe_3O_4 wasfabricated using precipitation technique. The final product was characterized to check the elemental composition and morphology by using XRD, SEM, EDX and TEM. The confirmed nanomaterial was dipped in water-soluble anticancer drug doxorubicin and loading of DOX onto nanoparticles was determined for twelve hours to be used as nanocarriers in further study.

Materials and Methods

Materials

Iron chloride hexa hydrate ($FeCl_3$. $6H_2O$, ACS reagent, 97-102%), Iron chloride tetra hydrate ($FeCl_2.4H_2O$, 99.99%), nickel chloride ($NiCl_2$, 99.99%),

cobalt chloride ($CoCl_2$, 99.99%), sodium hydroxide (NaOH, ACS reagent, ≥ 97.0%) and ethanol (C_2H_5OH, absolute reagent, 99.8%) were purchased from Sigma Aldrich and used without any further purification.

Synthesis of free and doped nano Fe3O4

The chloride salts of ferrous, ferric, nickel and cobalt were of reagent graded and used as precursors while sodium hydroxide (NaOH) was used as a solvent. DOX- doxorubicin was used as anti-cancer drug for loading onto fabricated nanoparticles. Firstly, an aqueous mixture of ferric and ferrous chloride salts (molar ratio 2:1) was prepared by dissolving in 50ml de ionized water. Secondly, another solution of 50ml of NaOH was dripped slowly to the above-prepared mixture in the air under vigorous stirring (1200 rpm). The reaction process continued at 20°C for 30 minutes. The black precipitate of Fe_3O_4 appeared in solution. These precipitates were thrice washed with de-ionized water and dried in an oven at 60°C as shown in Fig. 1. Two different iron salt solutions were prepared by adding 5% molar weight of dopants nickel and cobalt chloride salts in Step I while rest of the steps were followed in a similar manner (Kale & Torchilin, 2007). Hence, three different sample of nanoparticles i.e. Fe_3O_4, Ni-Fe_3O_4, and Co-Fe_3O_4, were obtained and readied to be used further in the experiment as in Table 1.

Table 1. Synthesis parameters.

Samples	Reactants		Product (NPs)
	Host Material	Dopant	
S1	$FeCl_3 \cdot 6H_2O$ + $FeCl_2 \cdot 6H_2O$	0	Fe_3O_4
S2	$FeCl_3 \cdot 6H_2O$ + $FeCl_2 \cdot 6H_2O$	$NiCl_2$	Ni: Fe_3O_4
S3	$FeCl_3 \cdot 6H_2O$ + $FeCl_2 \cdot 6H_2O$	$CoCl_2$	Co: Fe_3O_4

Incorporation of DOX

Three different solutions of prepared nano iron composite (50 mg) were immersed in 5ml of DOX solution (1 mg/ml) agitated continuously for 12 hrs at 24°C (Chen *et al.*, 2016).

The supernatant was well centrifuged as determined by UV spectroscopy to evaluate the incorporated DOX onto nanocomposites.

The decrease in the DOX concentration was in actual an amount of drug incorporated into the nanoparticles. This decrease in absorbance was evaluated frequently after each hour and studied the comparisons of drug loading between pure and doped nanoparticles.

Samples	Incorporation of DOX
S4	DOX- S1
S5	DOX- S2
S6	DOX- S3

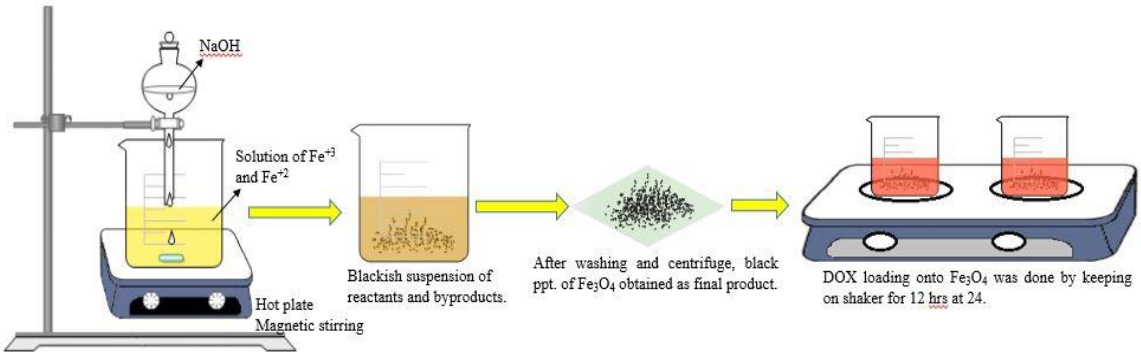

Fig. 1. Schematic of the synthesis process.

Characterization

The identification of phases and crystallite size of fabricated free and doped iron oxide nanomaterials was examined by PAN alytical X' Pert high score diffractometer (XRD) scanned in the range 2θ (i.e. 20°- 80°) using Cu Kα (λ = 1.5406°A) radiation.

To study the surface morphology scanning electron microscope (SEM) coupled with EDX System (model CARL-ZEISS EVO MA 15) and transmission electron microscope (TEM) & JEM 1230 were employed respectively. While EDX was done for identification of elements present and GENESYS 10S UV-Vis

spectrophotometer was used to record loading of medicine on nanoparticles after each hour.

Results and discussion

The observed diffraction patterns of Fe_3O_4, Ni- Fe_3O_4 and Co- Fe_3O_4, are comparatively presented in Fig 2. (a-c) respectively. All the characteristic reflection peaks in diffraction patterns (a-c) were well indexed by respective indices using respective JCPDS card numbers. It is evident that the host material is the magnetite phase of Fe_2O_3 which has a cubic structure with space group (227) 3d-m and lattice constant a = 8.360Å and planes are same in all patterns.

In Fig. 2a, the peak positions observed at 2θ = 29.98°, 35.30°, 43.23°, 53.54°, 57.16° and 62.72° with relative intensities corresponds to Fe_2O_3 with the JCPDS card no. 00-002-1035 and are assigned to their respective planes (220), (311), (400), (422), (511) and (440) (Akbarzadeh *et al.*, 2012).[17]

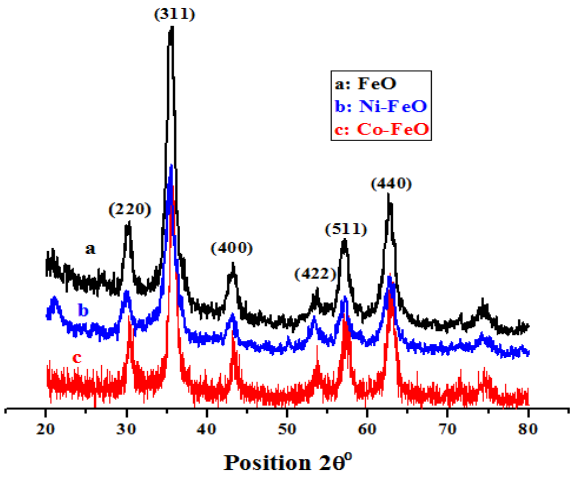

Fig. 2. XRD pattern of Fe_3O_4, Co-Fe_3O_4, and Ni-Fe_3O_4.

From broadening of XRD peaks, the measured average crystallite domain "d" is approximately 14.6nm in diameter by using Scherrer formula (Eq. 1) (Cullity BD & Stock, 2001),

$$d = {}^{0.9\,\lambda}/_{\beta \cos \theta} \cdot\cdot (1)$$

Where, θ is Bragg's angle and β is the full width of XRD peak at half maxima (FWHM), λ is X-ray wavelength).

The XRD pattern of Co and Ni-doped Fe_3O_4 are shown in Fig. 2 (b-c) respectively. In the graph (2b), the peaks position at 2θ = 30.16°, 35.59°, 43.25°, 53.55°, 57.17° and 62.72° along with relative intensities correspond to Co-Fe_2O_3 matched with the JCPDS card no. 00-002-1045 and are assigned to their respective planes (220), (311), (400), (422), (511) and (440).

The crystallite size of Co-Fe_2O_4 using Eq. 1 is around 23 nm in diameter. No characteristic peaks of impurity were seen. XRD patterns of nickel-doped iron oxide nanoparticles, shown in graph (2c), are satisfied by the JCPDS card no. 00-023-1119.

The peak positions at 2θ = 30.30°, 35.59°, 43.28°, 53.74, 57.2° and 62.77) are marked by reflection planes (220), (311), (400), (422), (511) and (440) respectively. The crystal size of Ni-Fe_2O_4 estimated using eq.1 is around 14.8nm. No characteristic peaks of any impurity were seen in all diffraction patterns.

Morphological studies of the synthesized Fe_3O_4 nanoparticles were performed by both TEM and SEM fitted with energy dispersive spectrophotometer (EDS) and are shown in Fig. 3 (a-b) at different magnificationand voltage of 20 kV.

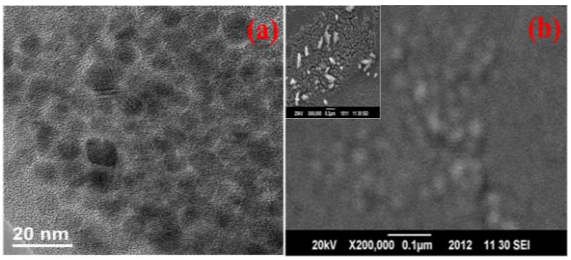

Fig. 3. TEM image of Fe_3O_4 (a) SEM micrographs of Fe_3O_4 (b).

TEM image of iron oxide NPs as shown in Fig. 3 reveals that the synthesized particles are around 10nm in size and are highly monodispersed with relatively narrow size distribution.

The elemental configurations of free, doped and DOX incorporated onto doped iron oxides, as examined by energy dispersive X-ray spectroscopy system (EDX), are shown in Fig. 4 (a-d) respectively.

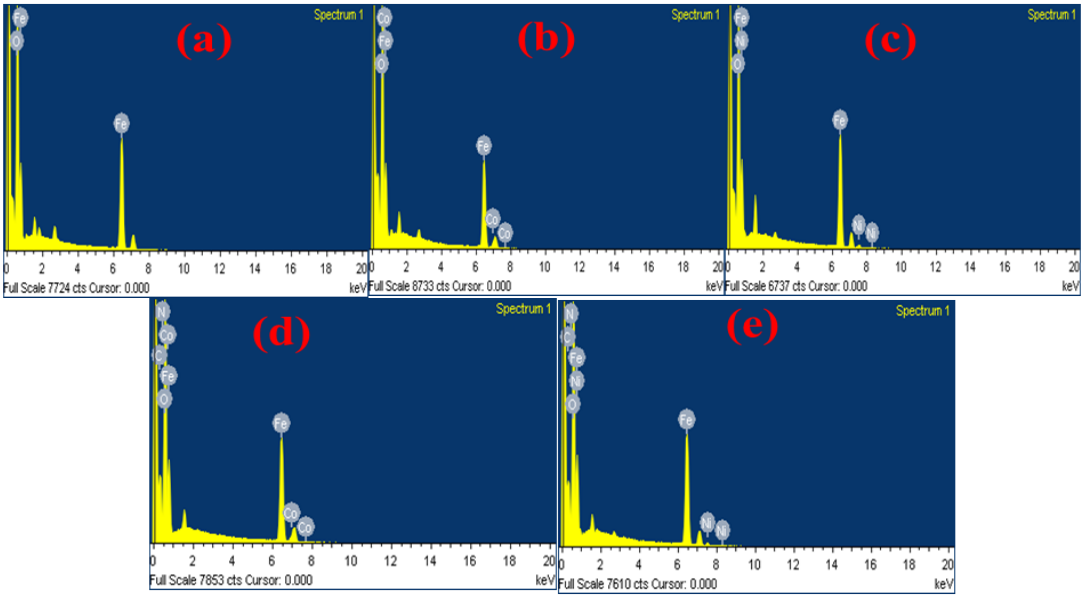

Fig. 4. EDX spectrum of Fe_3O_4 (a), Co- Fe_3O_4 (b), Ni- Fe_3O_4 (c), DOX: Co-Fe_3O_4 (d) and DOX: Ni-Fe_3O_4.

The strong signals of iron and oxygen elements are observed in all spectra, indicating the presence of iron oxide as the host material. The appearance of Co peak in Fig. 4(b,d) and Ni peak in Fig. 4(c,e) validates the doping effect in there spective host material. After loading of DOX on nanomaterials, the additional peak of carbon and nitrogen can be seen in the spectrum 4(d,e), confirms the loading of doxorubicin medicine. In case of pure Fe_3O_4nanoparticles (4a), thesame pattern was observed showing that no loading occurred.

Table 2. Elemental composition of iron oxide and its various composites.

Elements	S1 (Weight %)	S2 (Weight %)	S3 (Weight %)	S5 (Weight %)	S6 (Weight %)
Fe	69.64	67.76	62.49	55.77	56.31
O	30.36	29	33.6	30.69	30.4
C	0	0	0	7.87	9.67
N	0	0	0	3.21	5.78

An overviewof weight % age of the elements present in the samples S1, S2, S3, S5andS6 are provided in Table 2. From table 2 and Fig. 4 are indicating that the host material contains iron (~62-70%) and oxygen (~29-34%) for S1, S2 and S3.

The appearance of carbon and nitrogen in S5 and S6 indicate the occurrence of doxorubicin with a decrease (~20%) in iron and same oxygen quantity. The excess amount of C and N in S6 shows the maximum loading of DOX onto Co-Fe_3O_4.

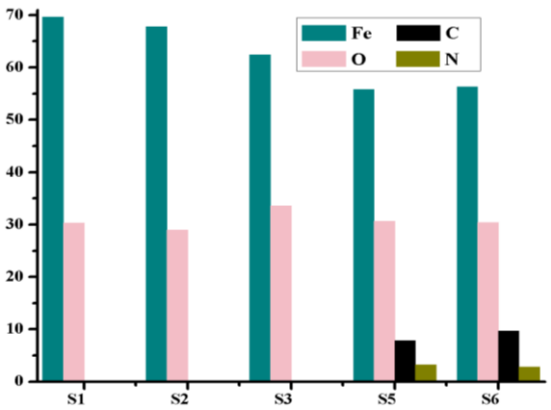

Fig. 5. Elemental composition of prepared specimens.

The incorporation of DOX onto different composites of iron oxides nanoparticles as observed by UV-Vis are shown in Fig. 6.

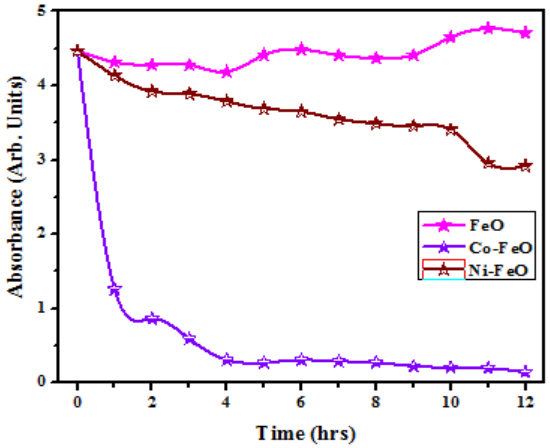

Fig. 6. Loaded spectrum of Fe_3O_4 with different composites.

Naked Fe_3O_4 has shown least absorbance over a period of 12 hrs as compared to doped ones, showing the least loading of DOX. On the other side, iron oxide with Co and Ni dopant has shown ~ 99.99% and 66% absorbance of DOX amount respectively. The particles synthesized in this route are very clear and symmetric having narrow size distribution revealed by TEM micrograph. Furthermore, the metallic core was prepared by reducing hematite or goethite and similar particles were prepared by a hydrogen reduction procedure preliminary with ferrihydrite, but the addition of the metallic dopants as ferrihydrite was formed in a solution or to the formed particles before hydrogen reduction (Chun, Baer, Matson, Amonette, & Penn, 2007). Moreover, high purity iron metallic core oxide nanoparticles were synthesized by a sputter aggregation process (Antony, Qiang, Baer, & Wang, 2006).

From XRD analysis, it is difficult to distinguish the dopants (Ni, Co) from host material (Fe_3O_4) nanoparticles as the doping may occur into lattice or into the surface of iron oxide nanoparticles and they have similar crystal structures (Koster, 1972). It was observed that for Co-doped samples up to 5%, the average particle size estimated from TEM didn't show any appreciable change as compared to pure γ-Fe_2O (S Chakrabarti, 2005). SEM analysis clearly defines the surface morphology of the particles which counter confirmed the nano size of the manufactured material. EDX results show the dopant peaks in its spectrum.

Loading efficiency (LE) and capacity (LC) of drugs were calculated by following equations 2 (Sabeti *et al.*, 2014) and 3 (Mohammad Hossein Mashhadizadeh and Mitra Amoli-Diva, 2012) respectively.

$$\% \text{ Loading efficiency of drug} = \frac{[Drug_{ini}]c - [Drug_{free}]}{[Drug_{ini}]} \times 100 \quad (2)$$

$$\text{Loading capacity of drug } \left(\frac{mg}{mg}\right) = \frac{[Drug_{ini}] - [Drug_{free}]}{[Drug_{carrier}]} \quad (3)$$

$Drug_{ini}$ is the initial amount (mg) of the drug, $Drug_{free}$ is the unbound drug remains in the supernatant and $Drug_{carrier}$ is the total amount (mg) of carrier.

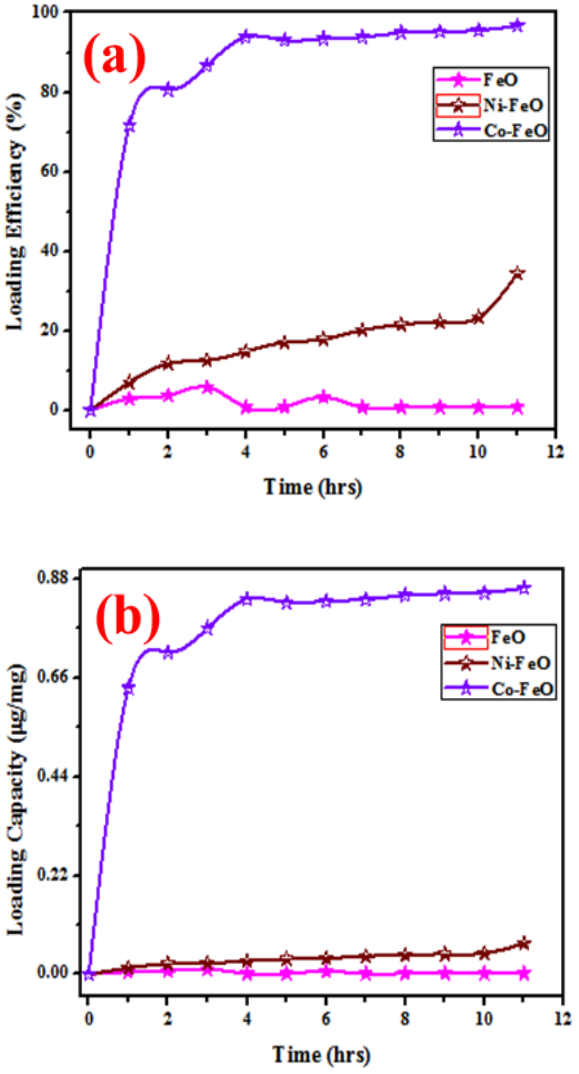

Fig. 7. Loading efficiency & loading capacity of nano composites of iron oxide.

Fe_3O_4 has shown low value of loading efficiency and capacity over 12 hrs as observed in Fig. 7 (a-b). The doped iron oxide has displayed high loading response in efficiency and capacity with the passage of time.

From Fig.s (7,8), a significant increase in loading efficiency and loading capacity with Co:Fe_3O_4 was found in first 5 hrs and this advantage slowdown in next same interval of time furthermore seems stable. This loading response is attributed to the doping concentrations.

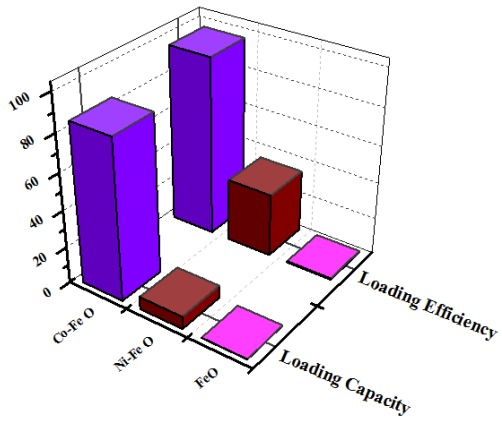

Fig. 8. Loading efficiency & loading capacity of the naked and doped material.

Fig. 8 depicts a comparison of loading efficiency and capacity of the naked and doped host material. The overview of the whole experiment suggests that the CoO is a promising candidate in pure as well as a dopant in other metal oxide.

It has been observed that Co doping not only increases reactivity but also modify reaction pathways (Lien & Zhang, 2007) and distribution of metal have to impact on the reactivity of particles (Zhang, 2003). Prepared particles were stirred in an aqueous solution of anticancer drug (DOX) to be diffused onto the particles. A lot of procedures are discussed which are responsible for drug loading such as surface charges, type of bonding laying among these materials. Considering these results, we can see that doping of Co play a much-unexpected role in the trapping of the drug onto the particles which is negligible without doping. The available binding site is a major factor, subsequently may be the forces which remain the conjugate firm (or loading), attractive forces like Vander Waals, play role in diffusion of drug (Javed *et al.*, 2015). During loading, we discover that pure Iron oxide diffused a little quantity of medicine on it while doping of Co enhances the diffusion property of pure iron oxide.

Kinetics Data Analysis

From above data it is observed that only doping of Cobalt in iron oxide gives fruitful results of medicine loading .The observed data is analyzed on the basis of Kinetics of adsorption mechanism, chemical reaction, mass transport processes, and diffusion rate r kinetic models.

Lagergren pseudo-first-order

The pseudo-first-order equation(Ho & McKay, 2000) can be written as

$$log(q_e - q_t) = log q_e - \frac{k_1}{2.303} t \qquad (3)$$

Where q_e and q_t are the drug a disorbed by Cobalt doped iron oxide nano particles at equilibrium state and at some time t respectively, k_1 is the lagergren rate constant of adsorption (1/min), by plotting graph of $log(q_e - q_t)$against t provides a linear relationship to calculate the value of k_1 and q_e from the slope and intercept of graph line respectively.

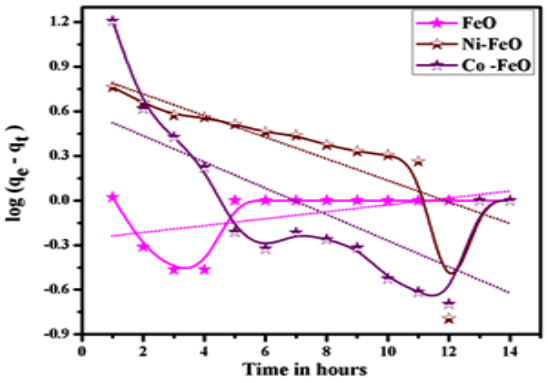

Fig. 9. Pseudo-first-order kinetic model.

Material	Q_e(mgg^{-1})	K_1(min^{-1})	R^2
FeO	10.38	0.253	0.966
Co-FeO	16.13	0.352	0.839
Ni-FeO	5.79	0.106	0.975

The validity of pseudo-first-order kinetic model was tested by the straight lines fitting as illustrated in Fig. 9. The values of the adsorption constant k_I and desorption mass at equilibrium state q_e found from pseudo first order linear plot doesn't match with experimental data at some points and have very small correlation coefficient (R^2 = 0.975) for Nickel doped iron oxide nanoparticals, suggesting that reaction deviate this model during ten to fourteen hours

Pseudo-Second-Order Model

The pseudo-second-order model [40] in linear form is

$$\frac{t}{q_t} = \frac{1}{k_2 q_e^2} + \frac{t}{q_e} \qquad (4)$$

The initial rate of absorption is

$$h = k_2 q_e^2 \qquad (5)$$

$$\frac{t}{q_t} = \frac{1}{h} + \frac{t}{q_e} \qquad (6)$$

Where k_2 represents the pseudo second-order adsorption rate constant (g/mg min). The values of q_e and k_2 can be determined from the slope and intercept of the graph of

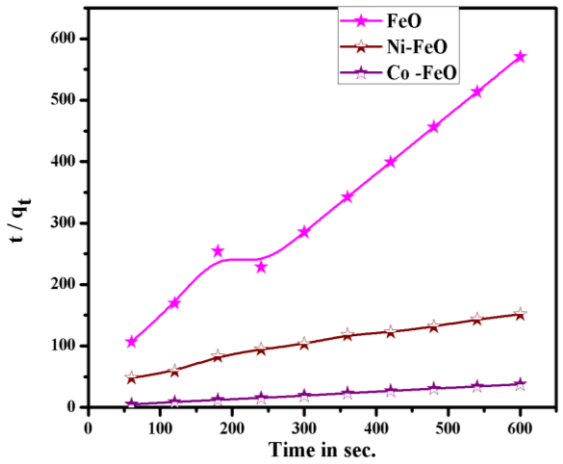

Fig. 10. Pseudo-second-order kinetic model.

Material	Qe(mg/g)	h (mg/g min)	K2(g/mg min)	R2
FeO	10.38	511370.09	4746.141	0.107
Co-FeO	16.13	91113.46	350.198	0.999
Ni-FeO	5.79	48764.51	1454.611	0.976

The plot of experimental value and application of the pseudo- second order model is shown in Fig. 10. This kinetic model good agreement with the experimental values. The values of the adsorption constant k_1 and desorption mass at equilibrium state q_e found from pseudo- second order linear match closely with experimental data and have coefficient (R^2 =0.999), suggesting that the this model is sensible to the adsorption processes of anticancer drugs on Cobalt doped Iron oxide involve chemical adsorption and may have ion exchange phenomenon (Liu *et al.*, 2017).

Elovich Model

The Elovich model (Chien & Clayton, 1980)can be presented as

$$q_t = \frac{1}{\beta} ln\alpha\beta + \frac{1}{\beta} lnt \qquad (7)$$

Where α is called initial adsorption rate (mg/gmin) and β is known as desorption constant (g/mg). The plot between q_t and lnt provides a linear relationship and α and $\beta$are the slope and intercept of the plot.

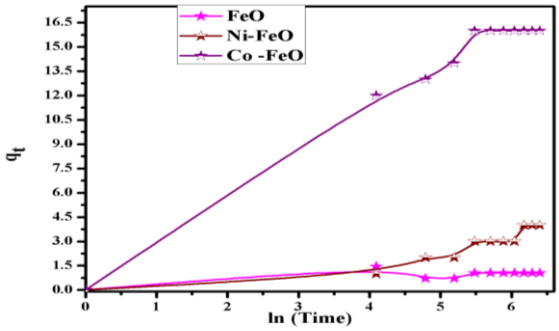

Fig. 11. Elovich model.

Material	α (mg/g)	β (g/mg)	R2
FeO	6.353	0.619	0.664
Co-FeO	3.374	0.396	0.974
Ni-FeO	1.357	1.645	0.860

Elovich model (Fig. 11) has almost agreement with experimental data having coefficient (R^2 =0.974), as it supports chemisorptions with heterogeneous adsorbing surfaces and the adsorption rate decreases with time as an increase in surface exposure (Arshadi, Amiri, & Mousavi, 2014). So it is clear that Elovich model doesn't match with experimental data at some points and have very small correlation coefficient (R^2 = 0.974) for Cobalt doped iron oxide nanoparticals,

Intra-Particle Diffusion Model

The intra-particle diffusion model (Cheung, Szeto, & McKay, 2007) is extensively used for adsorption studies where, k_i is the rate constants of intra-particle diffusion at stage i and can be determined by following equation:

$$q_t = k_i t^{1/2} + C_i \qquad (8)$$

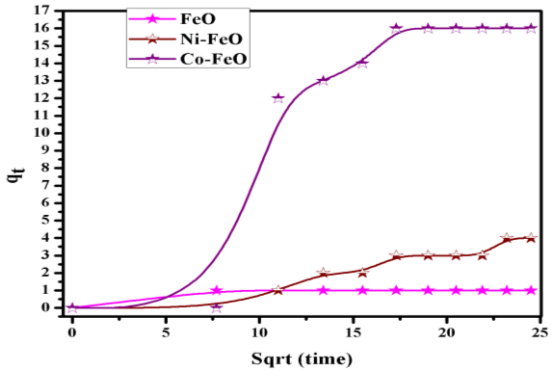

Fig. 12. The intra-particle diffusion model.

Material	k_I(mg/g.min1/2)	C_I(mg/g)	R2	k_{II}(mg/g.min1/2)	C_{II}(mg/g)	R2
FeO	0.648	5.800	0.871	0.648	5.800	0.871
Co-FeO	1.062	2.140	0.769	0.169	0.345	0.985
Ni-FeO	0.143	0.328	0.695	0.107	13.280	0.582

The intra-particle diffusion model predicts two rate controlling adsorption steps. The first step is sharper and does not pass intercept at origin as shown in Fig. 12 and showed that rate controlling step involves the boundary layer diffusion process. The second step is gradual with low diffusion rate due to low concentration of drug remain in solution. [45]. Here it can be assumed that The intra-particle diffusion model doesn't match with experimental data at some points and have very small correlation coefficient (R^2 = 0.985) for Cobalt doped iron oxide nanoparticals,

Conclusion

The application of magnetic nanoparticles as a carrier in drug delivery system is still defined by its biocompatibility and selective targeting to desired cells or tissue under the assistance of external magnetic field. Advances in current technologies and development in nano drug delivery systems have fast-tracked and headed to the creation of numerous nano-magnetic formulations like polymeric, metallic, non-metallic and liposomal nanoparticles. These novel delivery systems have increased the ability to carry drugs for which conventional therapy has shown limited efficacy. Technology will not only minimize invasive procedures but also reduce side effects to healthy tissues, which are two primary concerns in conventional cancer therapies (Sun *et al.*, 2008).

Acknowledgement

The authors are very thankful to Higher Education Commission-HEC for financial support in this research.

Conflict of interest: This manuscript has no conflict of interest.

Reference

Ahmd M, Rashid K, Nadeem M, Masood K, Ali S, Nafees M. 2012. A Simple Method to Prepare Aqueous Dispersion of Iron Oxide Nanoparticles and Their Biodistribution Study. Journal of Colloid Science and Biotechnology **1,** 201-209.

Akbarzadeh A, Samiei M, Joo SW, Anzaby M, Hanifehpour Y, Nasrabadi HT. 2012. Synthesis, characterization and in vitro studies of doxorubicin-loaded magnetic nanoparticles grafted to smart copolymers on A549 lung cancer cell line. Journal of Nanobiotechnology **10,** 46.

Antony J, Qiang Y, Baer DR, Wang C. 2006. Synthesis and characterization of stable iron-iron oxide core-shell nanoclusters for environmental applications. J.Nanosci.Nanotechnol **6,** 568-572.

Arshadi M, Amiri MJ, Mousavi S. 2014. Kinetic, equilibrium and thermodynamic investigations of Ni(II), Cd(II), Cu(II) and Co(II) adsorption on barley straw ash. Water Resources and Industry **6,** 1-17.

Chen C, Zheng P, Cao Z, Ma Y, Li J, Qian H. 2016. PEGylated hyperbranched polyphosphoester based nanocarriers for redox-responsive delivery of doxorubicin. Biomaterials Science **4,** 412-417.

Cheung WH, Szeto YS, McKay G. 2007. Intraparticle diffusion processes during acid dye adsorption onto chitosan. Bioresour.Technol **98,** 2897-2904.

Chien SH, Clayton WR. 1980. Application of Elovich Equation to the Kinetics of Phosphate Release and Sorption in Soils1. Soil Science Society of America Journal **44,** 265-268.

Chun CL, Baer DR, Matson D, Amonette JE, Penn RL. 2007. Characterizations and reactivity of metal-doped iron and magnetite nanoparticles. In pp. 536.

Cullity BD, Stock SR. 2001. Elements of X-ray Diffraction. In *Elements of X-ray Diffraction* (3rd ed., New York: Prentice-Hall.

De Jong WH, Borm PJ. 2008. Drug delivery and nanoparticles: Applications and hazards. Int J Nanomedicine **3,** 133-149.

Dilnawaz F, Singh A, Mohanty C, Sahoo SK. 2010. Dual drug loaded superparamagnetic iron oxide nanoparticles for targeted cancer therapy. Biomaterials **31,** 3694-3706.

Ho YS, McKay G. 2000. The kinetics of sorption of divalent metal ions onto sphagnum moss peat. Water Research **34,** 735-742.

Ito A, Shinkai M, Honda H, Kobayashi T. 2005. Medical application of functionalized magnetic nanoparticles. Journal of Bioscience and Bioengineering **100,** 1-11.

Jatariu A, Peptu C, Popa M, Indrei A. 2009. Micro- and nanoparticles--medical applications. Rev Med. Chir Soc. Med. Nat. Iasi **113,** 1160-1169.

Javed KR, Ahmad M, Ali S, Butt MZ, Nafees M, Butt AR. 2015. Comparison of Doxorubicin Anticancer Drug Loading on Different Metal Oxide Nanoparticles. Medicine **94,** 617-622.

Kale AA, Torchilin VP. 2007. Design, synthesis, and characterization of pH-sensitive PEG-PE conjugates for stimuli-sensitive pharmaceutical nanocarriers: the effect of substitutes at the hydrazone linkage on the ph stability of PEG-PE conjugates. Bioconjug. Chem **18,** 363-370.

Khoee S, Bafkary R, Fayyazi F. 2017. DOX delivery based on chitosan-capped graphene oxide-mesoporous silica nanohybride as pH-responsive nanocarriers. Journal of Sol-Gel Science and Technology **81,** 493-504.

Kim DK, Zhang Y, Voit W, Rao KV, Muhammed M. 2001. Synthesis and characterization of surfactant-coated superparamagnetic monodispersed iron oxide nanoparticles. Journal of Magnetism and Magnetic Materials **225,** 30-36.

Kohay H, Sarisozen C, Sawant R, Jhaveri A, Torchilin VP, Mishael YG. 2017. PEG-PE/clay composite carriers for doxorubicin: Effect of composite structure on release, cell interaction and cytotoxicity. Acta Biomater **55,** 443-454.

Koster E. 1972. Magnetic anisotropy of cobalt-doped gamma ferric oxide. Magnetics, IEEE Transactions on **8,** 428-429.

Lien HL, Zhang WX. 2007. Nanoscale Pd/Fe bimetallic particles: Catalytic effects of palladium on hydrodechlorination. Applied Catalysis B: Environmental **77,** 110-116.

Liu BY, Gong YJ, Wu XN, Liu Q, Li W, Xiong SS. 2017. Enhanced xenon adsorption and separation with an anionic indium-organic framework by ion exchange with Co2+. RSC Advances **7,** 55012-55019.

Mahmoudi M, Sant S, Wang B, Laurent S, Sen T. 2011. Superparamagnetic iron oxide nanoparticles (SPIONs): Development, surface modification and applications in chemotherapy. Advanced Drug Delivery Reviews **63,** 24-46.

Mohammad Hossein Mashhadizadeh and Mitra Amoli-Diva. 2012. Drug-Carrying Amino Silane Coated Magnetic Nanoparticles as Potential Vehicles for Delivery of Antibiotics. Journal of Nanomedicine & Nanotechnology **3,** 2155-7439.

Neuberger T, Sch Apf B, Hofmann H, Hofmann M, von Rechenberg B. 2005. Superparamagnetic nanoparticles for biomedical applications: Possibilities and limitations of a new drug delivery system. Journal of Magnetism and Magnetic Materials **293,** 483-496.

Parveen S, Misra R, Sahoo SK. 2012. Nanoparticles: a boon to drug delivery, therapeutics, diagnostics and imaging. Nanomedicine: Nanotechnology, Biology and Medicine **8,** 147-166.

Peer D, Karp JM, Hong S, Farokhzad OC, Margalit R, Langer R. 2007. Nanocarriers as an emerging platform for cancer therapy. Nat. Nanotechnol **2,** 751-760.

Sabeti B, Noordin MI, Mohd S, Hashim R, Dahlan A, Akbari Javar H. 2014. Development and Characterization of Liposomal Doxorubicin Hydrochloride with Palm Oil. BioMed Research International **2014,** 6.

Sun C, Fang C, Stephen Z, Veiseh O, Hansen S, Lee D. 2008. Tumor-targeted drug delivery and MRI contrast enhancement by chlorotoxin-conjugated iron oxide nanoparticles. Nanomedicine (Lond) **3,** 495-505.

Wilczewska AZ, Niemirowicz K, Markiewicz KH, Car H. 2012. Nanoparticles as drug delivery systems. Pharmacol. Rep **64,** 1020-1037.

Zhang WX. 2003. Nanoscale Iron Particles for Environmental Remediation: An Overview. Journal of Nanoparticle Research **5,** 323-332.